The Topografiner: An Instrument for Measuring Surface Microtopography

Russell Young, John Ward, and Fredric Scire

National Bureau of Standards, Washington, D. C. 20234

(Received 1 February 1972; and in final form, 29 March 1972)

A noncontacting instrument for measuring the microtopography of metallic surfaces has been developed to the point where the feasibility of constructing a prototype instrument has been demonstrated. The resolution of the preprototype unit is 30 Å perpendicular to the surface and 4000 Å in the plane of the surface. Inherent noise in the perpendicular direction corresponds to 3 Å or one atomic layer. By using a typical field emitter with radius of 100 Å, an ultimate limit of 200 Å would be expected for the horizontal resolution. Topographic maps of an infrared diffraction grating have been measured in order to demonstrate the performance of the instrument in measuring a well characterized surface. The instrument has been shown to conform to the Fowler–Nordheim description of field emission while spaced at the usual operating distances from the surface. When moved to within 30 Å of the surface, its performance is compatible with Simmons' theory of MVM tunneling. In the MVM mode, the instrument is capable of performing a noncontacting measurement of the position of a surface to within about 3 Å. The instrument can be used in surface science experiments to study the density of single and multiple atom steps on single crystal surfaces, adsorption of gases, and processes involving electronic excitations at surfaces.

INTRODUCTION

At present there is an abrupt separation between the "arts and sciences" of surface finish metrology on the one hand and surface science on the other. Surface scientists prepare and study surfaces of very small area which they believe either to be atomically perfect or to contain a small density of single or multiple atom steps (3–10 Å). The characterization of these surfaces is not supported by measurements of surface topography. Surface metrologists prepare and measure the profiles of large surfaces that are flat on the 25 Å level, without understanding the impact of physical and chemical surface processes on these measurements. It is hoped that the instrument discussed here will contribute to closing the gap between these two disciplines.

In the area of surface finish metrology, there has been increased demand for refined measurements. The finish of ceramic substrates for integrated circuits and single crystal silicon wafers is of vital interest to the growing electronics industry.[1] Instrument shafts and bearings utilizing extremely thin dry film lubricants require a high quality surface finish. The light scattering characteristic of reflecting optics in the ultraviolet region is determined by the surface finish of the coating.[2] The wavelength dependence of emissivity is dependent on the physical nature of the surface. Topographic mapping of diffraction gratings is a continuing difficult problem.[3] A pressing problem in surface science involves the characterization of surfaces used in surface science experiments.[4] It would be extremely useful to be able to characterize the so called "single crystal surfaces" on an atomic level. It is for the above reasons that the development of a new high resolution topographic mapping instrument called the Topografiner[5] (pronounced "toe-pog-rà-finer") is being undertaken.

This paper will give a general description of the Topografiner, associated electronic circuitry, and general performance. The application of field emission and MVM

tunneling will then be discussed with presentation of the first MVM tunneling results.

I. DESCRIPTION OF TOPOGRAFINER

Principle of Operation

A detailed discussion of the principle of operation of the field emission probe (ultramicrometer) has been given previously.[6] When a field emitter with a typical radius of 100–10 000 Å is brought close to a conducting surface while a constant current is being passed through the emitter, the electric field strength at the emitter surface is fixed by the Fowler–Nordheim (FN) equation (see Sec. IV). Laplace's equation then predicts the field strength everywhere between the emitter and the surface, and thus determines the relationship between the emitter-to-surface spacing (hereafter called the emitter spacing), and the emitter-to-surface voltage (hereafter called the emitter voltage). In the Topografiner, the voltage between the emitter and the surface is amplified and applied to a piezoelectric ceramic element on which the emitter is mounted. This forms a servo system which keeps the emitter a constant distance above the surface. The piezo voltage corresponds to the altitude of the surface. The Topografiner is equipped with two scanning piezo elements which sweep the emitter over the specimen surface in a pattern that can be used to generate a topographic map of the surface. The instrument actually scans a series of closely spaced profiles of the surface and plots them so as to give a three dimensional representation of the surface microtopography. The most important characteristic of the instrument is that the probe does not contact the surface and cause damage.

The present realization of the instrument is shown in Fig. 1. The specimen is mounted between two heavy copper clamps which are spring loaded in order to hold the thin
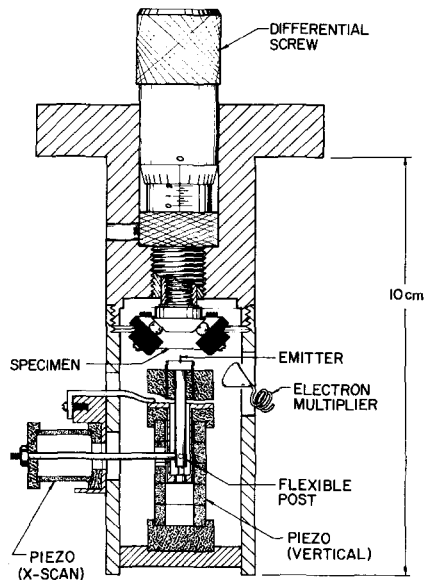
FIG. 1. Present realization of the Topografiner. The differential screw is used as a coarse adjustment to bring the specimen close enough to the emitter so that it is within the range of the vertical (Z) piezo. The X-scan piezo deflects the emitter support post so as to scan the emitter in one direction. The orthogonal (Y) piezo is not shown. The specimen is clamped between copper blocks to permit heating. An electron multiplier permits detection of secondary electrons.

sheet specimens (for example, replicas) taut. An electrical current may be passed through thin specimens in order to heat them for cleaning. Thick specimens are not heated. A differential screw moves the specimen assembly through a 0.254 mm excursion by deflecting a thin welded diaphragm at the end of the screw. The emitter support assembly consists of two 1.0 mm molybdenum rods clamped in a boron nitride holder. The tungsten emitter, which has been electrochemically etched from a ~0.1 mm wire, is spot welded to two 0.125 mm molybdenum bridges between the rods in order to heat the emitter for cleaning. The two bridges support the emitter rigidly. The emitter assembly, mounted on a flexible post supported by the vertical piezo, is moved perpendicular to the specimen surface by the vertical piezo. The piezo itself consists of a stack of five piezo disks 4.8 mm thick spaced by gold wire rings with alternate rings electrically connected. The gold ring construction prevents the entrapment of gases, is vacuum compatible, and flows sufficiently at the point of contact to distribute the force uniformly around the circumference of the disks. The vertical stack is clamped with two phosphor bronze leaf springs.

The X and Y scan piezos are cylinder expanders which provide greater deflection sensitivity at the expense of an increase in hysteresis. They deflect the post at a point one-fifth of the total distance from the base to the emitter, resulting in an emitter scanning distance of about 0.0076 mm. The X and Y piezos will soon be replaced with a linear stack similar to the vertical piezo. The electron

multiplier, which detects secondary electron emission from the specimen surface, will be discussed later.

The entire assembly in Fig. 1 is connected, by means of the vacuum flange at the top, to a vacuum system pumped by a combination titanium sublimation and ion pump. A mechanical pump was used during initial stages of evacuation but is disconnected during measurements. The instrument is mounted on a low vibration table that consists of a 750 kg mass supported by three arms, each of which is mounted on a rubber diaphragm air mount with an expansion chamber and aperture. The whole system has a vertical period of about 1 Hz and is critically damped. The vacuum chamber is surrounded by an acoustical shield. Over most of the frequency range the sound pressure amplitude, as measured with a wide range crystal microphone, is about one order of magnitude below the level in the room. Vibrations at the vacuum system are below the noise level of the accelerometer used to test the effectiveness of the low vibration mount and do not exceed a few tens of angstroms. Also, as indicated in Fig. 1, the emitter and specimen assembly are rigidly mounted to the same flange to avoid relative motion.

A number of parameters determine the basic sensitivity of the Topografiner. A relationship has been found that connects the minimum detectable displacement for an emitter carrying a constant current, to the emitter spacing, emitter radius, and the minimum detectable change in emitter voltage.[6] Assuming that the emitter voltage can be
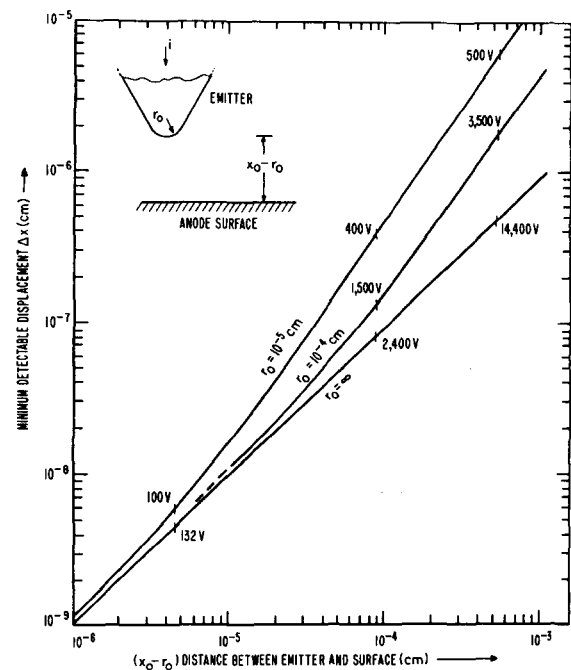
FIG. 2. Minimum detectable displacement of the emitter if the emitter voltage can be measured to one part in 10^3. In the present application, the emitter to anode voltage (marked on the curves) is about 50–100 V where the minimum detectable distance is independent of emitter radius, R_e.

measured to one part in 10^3, the minimum detectable displacement is shown in Fig. 2. For a typical emitter spacing of 200 Å, the theoretical minimum detectable displacement is 0.2 Å, regardless of the emitter radius. In order to remove the effects of ambient gas on system noise when a tungsten emitter is used, it has been necessary to employ a vacuum of about 4×10^{-10} Torr for quiet operation. Emitters that are less sensitive to ambient gases should relax this requirement. A topographic map of a 180 line/mm diffraction grating replica is shown in Fig. 3(a). Figure 3(b) is a map of a disturbed region of the same grating recorded with a memory oscilloscope in place of the X-Y recorder. The total recording time was 9 min, about $\frac{1}{10}$ what would be required with an X-Y recorder.

Electronic Circuitry

The block diagram for the Topografiner is shown in Fig. 4. The X and Y piezos derive their scan voltages from high voltage power supplies programmed with electronic function generators. The Z piezo is part of the servo loop which will now be described in some detail.

Servo Loop

The elements of the servo loop, which keeps the emitter a constant distance from the surface, include a constant current power supply, a 2000 V operational amplifier, an RC element consisting of the piezo capacitance and an interchangeable resistance, the piezo itself, and the field emission probe device.

In the circuit diagram for the constant current power supply shown in Fig. 5, the field emitter is represented by the variable load resistor R_L. The voltage drop across the current sensing resistor, R_K, resulting from the load current through it, is compared with a reference voltage produced by the current control potentiometer, R_C, at the input of the differential operational amplifier, A_1. The amplified difference error voltage is applied to the base of the 2N4298 transistor which in turn supplies the controlled load current. It is the voltage across the load, R_L, that serves as the control voltage for the servo loop to be described in the following paragraphs. However, since R_L is a very high resistance, a proportional output voltage is made to appear across a more practical lower resistance, R_0. Also, for operating load currents smaller than 10^{-6} A, the branch containing resistor R_0 carries the excess or difference between the load current and the 10^{-6} A cutoff current of the output transistor. With this feature the supply can deliver a constant current from 10^{-2} to 10^{-10} A with up to 300 V compliance. The voltage across R_0 can also be used as a guard voltage to prevent leakage current in the wiring to the load, R_L.

In the circuit shown, the response time for a change of current at the load due to a change of reference voltage at
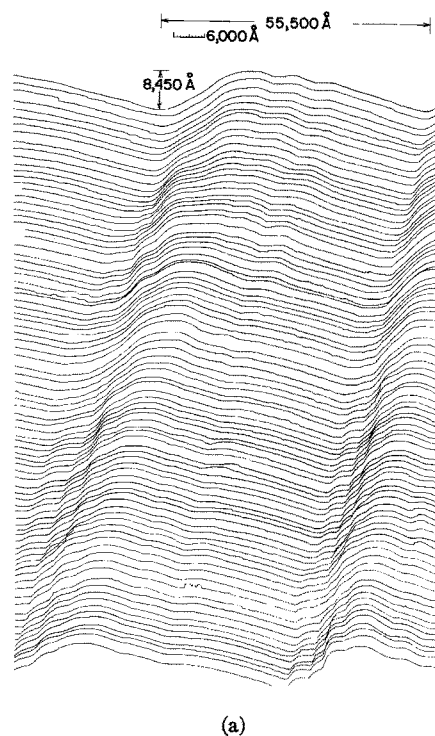
(a)

(b)

Fig. 3. (a) Topographic map of a 180 line/mm diffraction grating replica. This map was made with the instrument in Fig. 1 using an X-Y recorder. Note the rippled surface at the base of the groove which may have been caused by ruling instrument chatter or replica removal. Details of the diamond tool used in the ruling engine are evident. The emitter was kept about 200 Å above the surface during these runs. (b) Topographic map recorded on a memory oscilloscope of a disturbed region of the same grating as (a). The vertical magnification is about twice the horizontal magnification. The contrast is reversed for easy comparison with (a). The close spaced profiles give a highly desirable pictorial representation of the surface topography. Mapping time—9 min.
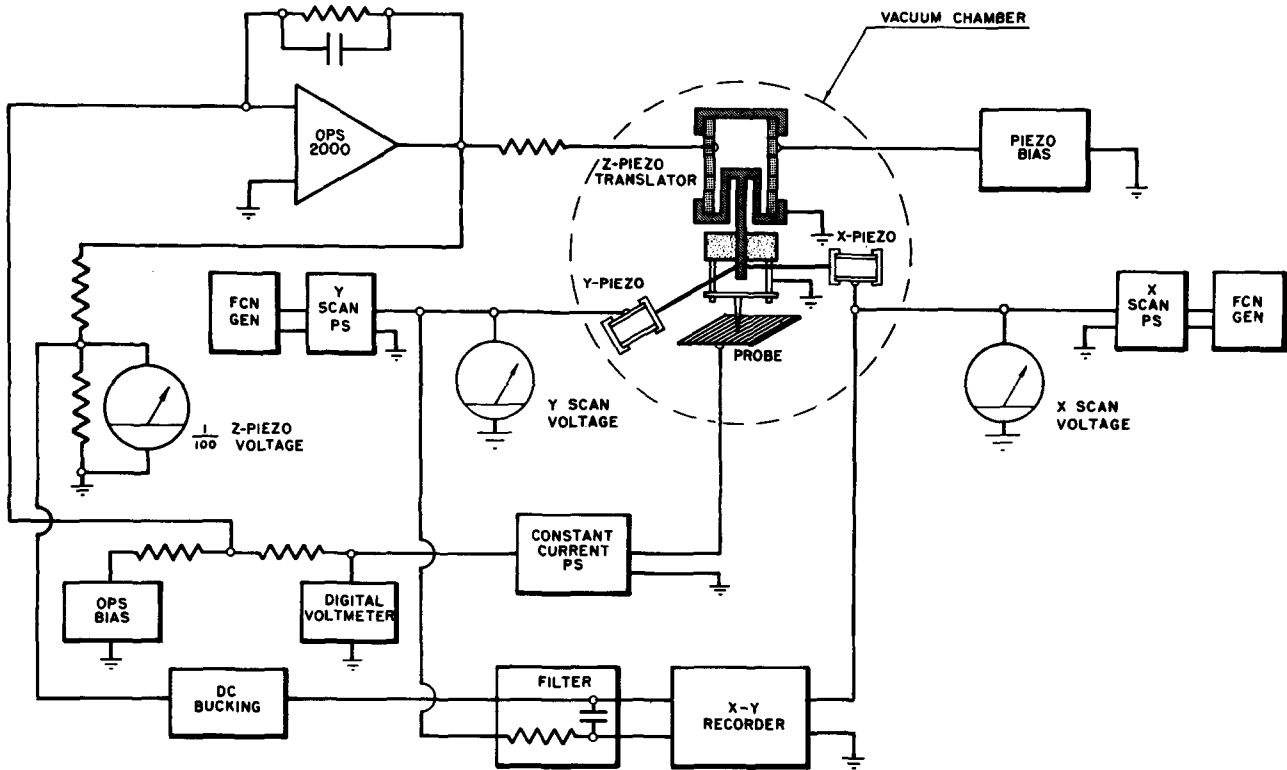
FIG. 4. Block diagram for the Topografiner electrical circuitry. The $X-Y$ recorder is frequently replaced with a memory oscilloscope which results in rapid scan rates with somewhat reduced fidelity. The OPS bias permits positioning the emitter at an appropriate distance from the surface. Details of the servo loop are discussed in the text.

R_c is dependent on the product of the load resistance, R_L, and its shunt capacitance, C_L. For example, if the load resistance has a value of 10^9 ohms and a shunt capacitance of 10 pF, the time constant would be 10^{-2} sec. For an output of 100 V, the slewing rate would be about 5 V/msec. A sizable improvement in this response time can be achieved by a compensating capacitor across R_K.

FIG. 5. Circuit diagram for the constant current power supply. With the indicated components, the constant current can be varied between 1×10^{-8} and 5×10^{-7} A. By changing R_K the current may be varied over a range from 10^{-2} to 10^{-10} A with up to 300 V compliance. C is the low voltage power supply common.

However, in the intended application, the response time of interest is not that due to a change in reference voltage at R_C, but rather due to a parameter associated with the load resistance change. For this case, the improvement in response time would have to be dealt with by some form of feedback circuitry that can directly nullify the shunt capacitance, C_L. Such constant current supplies, now under test, have response times of about 1 msec.
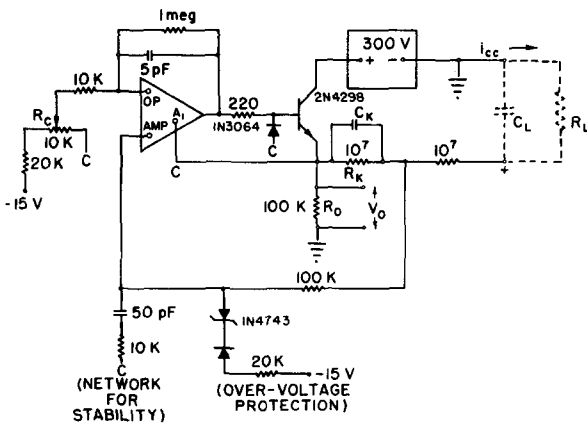
The 2000 V operational amplifier has a gain of 40 and a frequency response flat from dc to 4000 Hz. This amplifier drives the piezo unit through a resistor which, in combination with the inherent piezo capacitance of 1000 pF, determines the time constant of the servo loop. The corner frequency for the present system is $f = (2\pi RC)^{-1} = 80$ Hz. The design goal for the system corner frequency is 2 kHz for reasons that will be discussed later. The present system has been purposely limited to 80 Hz because of mechanical resonances in the piezo stack structure, supporting members, and connecting wires. These mechanical resonances, which must be eliminated in the next generation of the instrument, cause phase shifts and thus servo loop instabilities.

A fundamental difficulty with the servo loop design in this instrument is caused by the variable gain term introduced by the field emitter characteristic. The gain of

the servo loop is given by

loop gain= (gain of CCPS)× (gain of OPS)

$$\times \text{(gain of piezo)}\times \text{(gain of FE)}$$

$$=1\times 40\times \frac{13\ \text{Å}}{\text{V}}\times \frac{0.2\ \text{V}}{\text{A}}=104.$$

The last term, gain of the field emitter, increases by a factor of 60:1 as the emitter is moved from far away to the specimen surface. The emitter gain is determined by the slope of the emitter voltage vs distance curve. Figure 6 is a plot of the theoretical slope of the emitter voltage curve as a function of emitter voltage with a number of emitter spacing values indicated. The corresponding servo loop gain is also given. The details of the calculation used to obtain this curve are given in a later section of this paper. The gain rises most steeply in the region where the instrument presently gives its best resolution, i.e., at about 50 V. In the low voltage region just to the left of the knee in the curves, the gain exceeds 700× because of vacuum tunneling, which will be discussed later. The instrument is never operated in this region due to the instability resulting from the high gain and because the emitter is only tens of angstroms from the surface in this region. It is important to note that the error involved in measuring the vertical position of the surface due to the properties of the servo loop varies inversely with the loop gain. Thus, the error is less than 1% close in and is typically 4% under usual operating conditions where the emitter voltage is about 50 V. It is anticipated that the next design will
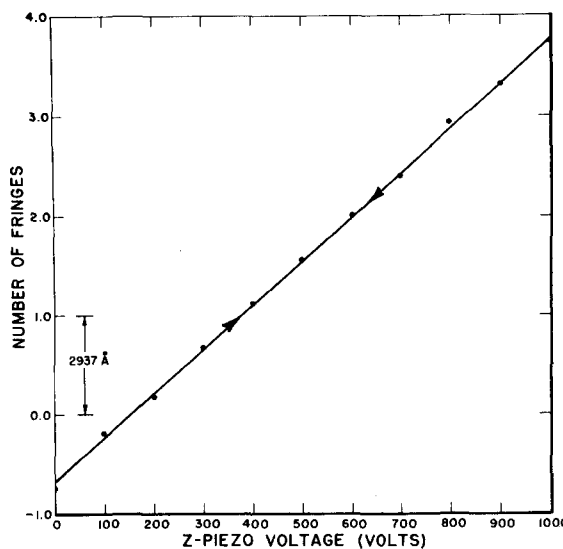
Fig. 7. Strain–voltage characteristic for the Z piezo stack. Type PZT-8; five-disk stack; d const.$=13.0$ Å/V. The displacement of the top of the stack was measured in an interferometer. The ordinate is given in terms of the number of half-wavelength shifts resulting from the applied piezo voltage. Note the absence of hysteresis.

incorporate a variable gain amplifier to compensate for the variable emitter gain and will hold the vertical error to about 1%.

The precision and linearity of the vertical readout depend on the gain of the servo loop, as discussed above, and the properties of the piezo stack. After final assembly, the stack was mounted in an interferometer and calibrated *in situ*. As can be seen in Fig. 7, the PZT-8 material is linear and has very little hysteresis.

II. INSTRUMENT PERFORMANCE: RESOLUTION AND REPRODUCIBILITY

System Noise

The two principal sources of noise in the Topografiner electromechanical servo system are electronic noise and mechanical vibration. The field emission process itself generates electronic noise due to fluctuations in the emission current density over the surface of the emitter. These changes appear as emitter voltage fluctuations since the emission current is constant. They are due to migration of atoms over the surface of the emitter and can be thermally activated or they can be caused by the ionization of a gas phase atom or an atom which has been adsorbed on the anode giving up the energy gained in the field (3×10^7 V/cm) to adsorbed atoms on the emitter surface. This source of noise can be minimized by using emitter materials that are less sensitive to adsorbed gases or which are less apt to adsorb gas atoms. The precautions taken to minimize noise due to mechanical vibrations have already been discussed.
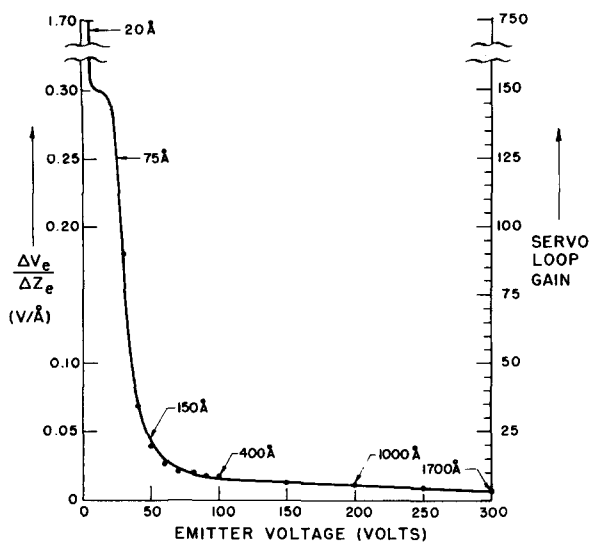

Fig. 6. Dependence of servo loop gain on emitter voltage. The gain of the servo loop depends on the slope of the emitter voltage vs emitter spacing curve ($\Delta V_e/\Delta Z_e$). The emitter spacing is indicated at several points along the curve. The drastic increase in servo loop gain at very low emitter voltages will be discussed in the section on MVM tunneling.
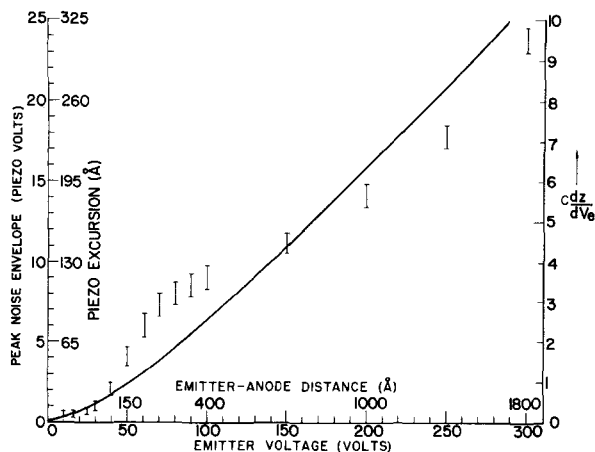
FIG. 8. Comparison of peak noise voltage (solid curve) with reciprocal of servo loop gain $[=Cdz/dV_e$ (data points—error bars)$]$ as the emitter voltage (emitter spacing) is varied. The ordinate on the left is also labeled in terms of the peak piezo excursion associated with the noise. As expected, the noise increases approximately as the reciprocal of the servo loop gain. The deviation at about 100 V is not understood.

If a voltage fluctuation occurs at the emitter, then the servo loop will apply sufficient voltage to the vertical piezo to move the emitter to compensate. If the emitter is far away from the surface, considerable motion may be necessary to compensate for the fluctuation, whereas a small motion is sufficient to compensate close in. Thus, one would expect the servo system gain variation, which was discussed above, to contribute inversely to the noise level in the system. In other words, for a given emitter voltage fluctuation the peak noise voltage should vary as dZ/dVe. Figure 8 shows a comparison of the experimentally measured peak [i.e., $(P-P)/2$] noise with the measured dZ/dVe data points. The ordinate also is labeled in terms of the vertical piezo excursion necessary to compensate for the voltage fluctuation and the abscissa is labeled in terms of emitter spacing. It is clear that a major contribution to system noise stems from variable servo system gain. It is also clear that both minimum noise conditions and best resolution occur when the emitter is close to the anode surface, a fortunate coincidence.

Noise resulting from vibration of the emitter or anode should not depend appreciably on emitter spacing. It has been observed that after the emitter is cleaned by heating, the noise is minimal, slowly increasing with time. Noise is independent of current density over the range available from the constant current power supply discussed above. After the emitter accidentally contacts the specimen surface the system noise level is very low, presumably due to cleaning of the emitter surface. The noise then slowly increases with time, perhaps reaching equilibrium after an hour or so.

In order to obtain a measure of the minimum attainable system noise with a tungsten emitter, the vertical piezo voltage was recorded as a function of time after the emitter

had contacted the surface. The emitter was slowly drifting toward the surface at about 2.5 Å per second due to thermal expansion. The results are shown in Fig. 9. It is necessary to choose a condition where the emitter is moving smoothly toward the specimen in order to be sure that the low noise is not due to physical support between the emitter and the surface due, for example, to oxide fragments. Figure 9 demonstrates that under quiet electrical conditions the system noise is less than 3 Å, which corresponds to one atom layer on the specimen surface. It should therefore be possible to improve the present system until this level is achieved. Studies are now under way testing the noise at the surface of Ge and Si emitters which are known to be less susceptable than tungsten to ion sputtering noise. Oxide coated and noble metal emitters are also under consideration.

The resolution in the plane of the surface, called the horizontal resolution, is determined by the radius of the emitter when the emitter is scanned very close to the surface. For example, in the two dimensional approximation, if the emitter were scanned over a very sharp peak, say a delta function, the vertical piezo output would be shaped like a lump of width approximately equal to twice the emitter radius. On the other hand, a depression about twice the size of the emitter radius would produce a sharp indentation in the measured profile and represents the smallest depression which can be detected with confidence. Thus, one can say that to first order the resolution of the Topografiner is limited to twice the emitter radius. This is typical of stylus instruments. Since 100 Å radius emitters are produced fairly easily for use in field emission microscopes, it would seem that 200 Å horizontal resolution is a reasonable goal for the Topografiner. All of the emitters used in the present study have had radii in excess of 1000 Å even though sharper emitters were installed in the instrument. The reasons why the emitters became blunt are not clear. Preliminary studies suggest that the ion pumps, which are used because they are free of vibration, have powerful electrical discharges in the early stages of pumpdown. The radio frequency fields associated with this discharge may cause excessively high currents to flow through the emitter, causing emitter rupture and blunting. This effect is presently under study.
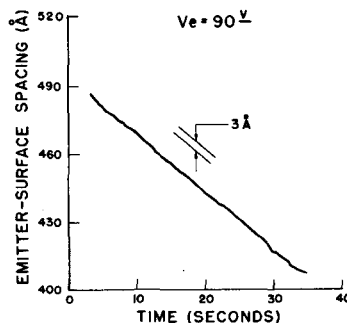

FIG. 9. Demonstration of low noise performance of the system. After the emitter had contacted the surface, the emitter position (Z piezo voltage) was recorded as a function of time. The emitter drifted slowly toward the surface (about 2.5 Å/sec) due to thermal instability. Note that the peak to peak noise did not exceed 3 Å (less than the height of a single atom step).

Resolution and reproducibility can be demonstrated by the magnified profile of a diffraction grating replica surface (shown in Fig. 10). The emitter traced the surface one and one-half times, jumped slightly to the right and completed two and one-half traces. Careful measurement of the tracking of these traces either before or after the jump shows that vertical position is reproducible to within ± 20 Å. Experience with the instrument has shown that 20–30 Å reproducibility is typical performance. Until it is possible to employ atomic steps of known height to determine the vertical resolution, the reproducibility will be assumed to be the achieved resolution. The horizontal resolution is about 4000 Å implying an emitter radius of about 2000 Å. Repeated traces over the same region continue to produce the same traces, as shown in Fig. 10, demonstrating that the surface is not damaged by the high current density, low energy, electron beam.

Decreasing the distance between the emitter and the surface has a very strong influence on both the vertical and horizontal resolution. Figure 11 shows the effect of decreasing the emitter spacing in three steps from about 400 Å to about 180 Å. The decrease in noise is obvious. The improvement in the detail of the profile is due to the fact that the field strength at the emitter surface is a result of the average distance to the specimen surface over an area about the size of the emitter for close in scans. As the emitter is moved farther from the surface, the area of the specimen over which the average is taken increases as the square of the emitter spacing. Thus, features like the ridges and grooves of the diffraction grating replica in Fig. 11 contribute appreciably to the effective specimen area only when the spacing is small. By adjusting the OPS bias, it is possible to withdraw the emitter from the surface, scan quickly over a region to get a rough idea of the topography, then zoom in to plot a detailed topographic map.

The minimum emitter size is ultimately limited by the power density associated with the impingement of the electron beam on the specimen surface. Oosterkamp has

FIG. 11. Magnified profile of a defective region on the same surface as Fig. 10. Note the strong influence of emitter spacing (indicated just below emitter voltage V_{cc}) on the noise and the detail resolved in the surface structure. Topographic maps are usually taken at about 50–60 V. $R_e \sim 1300$ Å.

shown[7] that refractory metal surfaces can withstand power densities of 10^8 W/cm² over a 1000 Å diam spot without melting. The tolerable power density is inversely proportional to the spot diameter. If an arbitrary limit of 10^6 W/cm² is set as a conservative limit in the Topografiner, a 125 Å emitter operating at 50 V can safely deliver 10^{-7} A to the anode. At present, typical operating currents are somewhat less than 10^{-7} A.

When the emitter accidentally contacts the surface, the stored energy in the capacitance of the constant current lead can cause severe damage to the emitter. For example, an emitter with a radius of a few hundred angstroms adjacent to an anode with a capacitance of 10 pF at a potential of 50 V will deliver about 10^{10} W/cm² to the emitter and anode if the discharge time is 10^{-7} sec. This is an unacceptably high power density at the emitter surface and will result in blunting and emitter welding to the specimen surface. Sudden emitter contact with the specimen is caused by a shock impulse to the instrument, either mechanical or acoustical, or by the presence of a particle of oxide or dust on the surface which temporarily holds the emitter away from the surface during a scan. The latter effect can be observed as a very disturbed region in the topographic map. One such disturbance is seen toward the bottom of Fig. 3(a).

III. SECONDARY ELECTRON EMISSION

When the field emitted electrons strike the specimen a large number of secondary electrons are released. The number emitted in a particular direction depends on the slope of the surface, its crystallographic orientation, its work function, the presence of adsorbed layers on the surface, and the energy of the incident electrons. Since there is an extremely strong electrostatic field at the surface, electrons tend to return to the anode, resulting in a strong dependence of the measured yield on emitter spacing (emitter voltage). The secondary electrons which escape are collected by a positively biased Channeltron
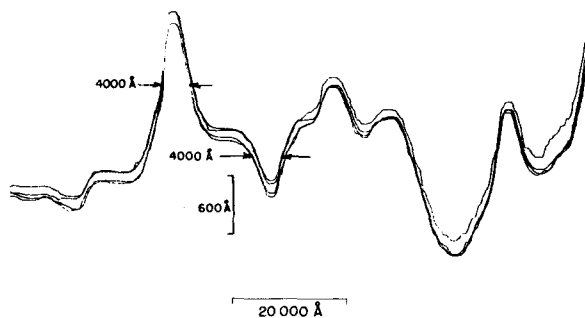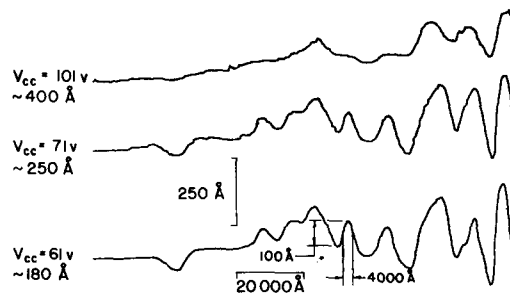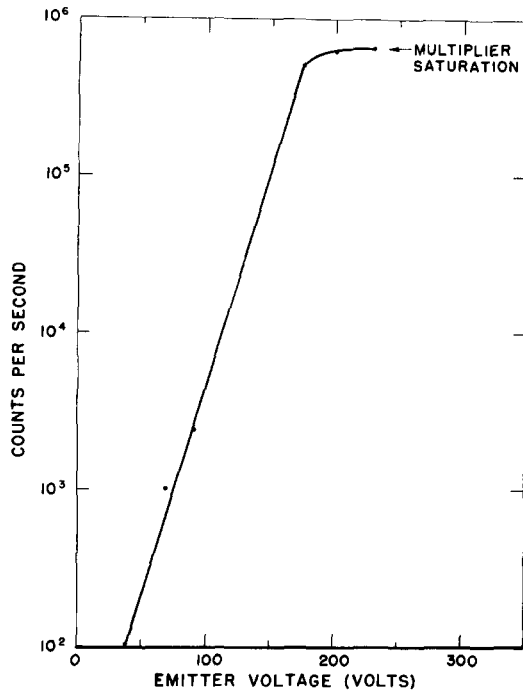

FIG. 10. Magnified profile of a small portion of a platinum replica of a 570 line/mm glass diffraction grating. Note that the emitter traced the surface one and one-half times, jumped slightly, and traced another two and one-half times. The vertical reproducibility before and after the jump is between 20 and 30 Å. Horizontal resolution is about 4000 Å. $V_{cc} = 46$ V; emitter–surface ~ 140 Å; $R_e \sim 2000$ Å.

FIG. 12. Number of secondary electrons detected per second as a function of emitter voltage for a total emission current of about 3×10^{-8} A. In the high resolution region ($V_e < 100$ V) the counting rate is only 10^3 count/sec. In order to increase this rate it will be necessary to add focusing electrodes near the emitter.

FIG. 13. Secondary electron profiles as emitter is scanned over the surface of a thermally etched T_a strip. The main features are quite reproducible. $V_e = 160$ V; $V_{mult} = 2800$ V; $V_{horn} = 100$ V; $\sim10^3$ counts/sec.

multiplier located nearby, as shown in Fig. 1. The number of electrons counted as a function of emitter voltage (spacing) is shown in Fig. 12. When the emitter is scanned over the surface, the output of the multiplier can be used to Z modulate an oscilloscope and obtain a secondary electron emission picture of the surface, similar to a scanning electron microscope picture. Very preliminary pictures show crude light and dark areas. The secondary electron emission profiles shown in Fig. 13 demonstrate the feasibility of making such pictures. Since it is anticipated that electron beam diameters as small as a few hundred angstroms will be obtained, it is hoped that high resolution images will ultimately be obtained at the same time the surface topography is mapped.

IV. COMPARISON OF EXPERIMENTAL RESULTS WITH FOWLER-NORDHEIM THEORY

It is important to demonstrate that the operation of the Topografiner is indeed consistent with the Fowler–Nordheim equation. In the Topografiner, it is possible to move the emitter with respect to the anode while measuring current and voltage. By combining the Fowler–Nordheim and Laplace's equation, it should then be possible to obtain one more relationship between emitting area, current, voltage, and work function, and thus perform a more stringent test of the Fowler–Nordheim theory than has previously been possible. The results reported
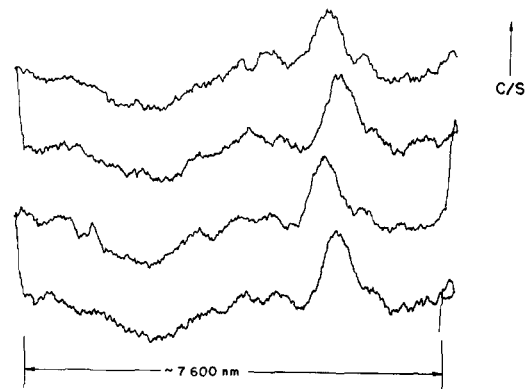
here will not constitute such a test since the instrument and experiment were not designed to perform this function. However, they are of sufficient quality to compete with previous tests and are of interest since this approach is quite different from previous ones. In the following paragraphs, Laplace's equation will be used to obtain a relationship between emitter voltage and emitter–anode (specimen) spacing. This will determine the emitter radius. Similar measurements very close to the surface then permit determination of the field strength at the emitter. This will then be combined with Fowler–Nordheim measurements to verify the Fowler–Nordheim theory.

Russell assumed that the emitter was a hyperboloid and used the prolate spheroidal coordinate system to obtain solutions of Laplace's equation.[8] The appropriate diagram for the present calculation is shown in Fig. 14 where lines of constant ξ are electric field lines, surfaces of constant η
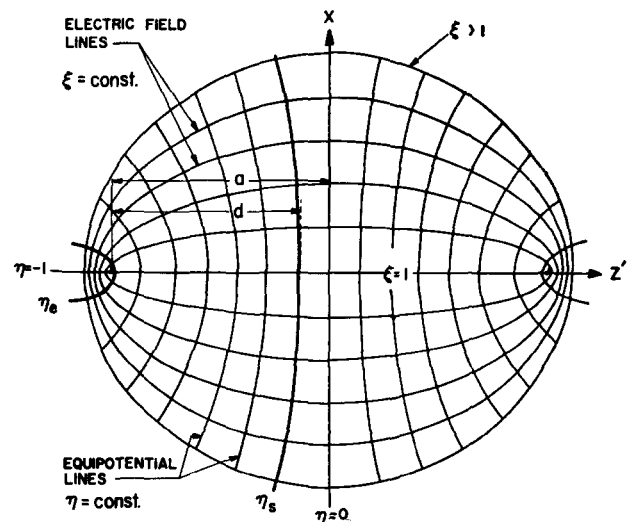

FIG. 14. Prolate spheroidal coordinate system. η_e is the equipotential contour corresponding to the emitter surface, $\eta = 0$ corresponds to the specimen or anode.

are equipotential surfaces, η_e is the equipotential corresponding to the emitter surface, and $\eta = 0$ is the flat anode surface. Russell has shown that the potential in this coordinate system is[8]

$$V(\eta) = \frac{V_e}{\ln[(1+\eta_e)/(1-\eta_e)]} \ln\left(\frac{1+\eta}{1-\eta}\right), \quad (1)$$

where V_e is the potential between the emitter and anode. The relationship between R_e, the emitter radius at the apex, a, the distance between the focus of the hyperboloid and the $\eta = 0$ surface, and η_e is given by

$$R_e = -(a/\eta_e)(1-\eta_e^2). \quad (2)$$

If Z_e is the rectangular coordinate distance between the emitter and the anode and $Z_e = a\eta_e$, then the field at the apex is

$$E|_{Z=a\eta_e} = \frac{2V_e}{a\ln[(1+\eta_e)/(1-\eta_e)]} \frac{1}{(1-\eta_e)^2} \equiv E_0. \quad (3)$$

Solving (2) for η_e, substituting in (3) and solving for V_e, the following relationship between emitter voltage and spacing is obtained:

$$V_e = (E_0 a/2)[1-\eta^2] \ln[(1+\eta_e)/(1-\eta_e)]. \quad (4)$$

Pairs of values for V_e and Z_e can be calculated by substituting values for E_0 and R_e in Eqs. (4) and (2), varying a, and recalling that $Z_e = a\eta_e$. The results of one such calculation are shown in Fig. 15 where the abscissa is the log of the emitter to anode spacing in units of R_e and the
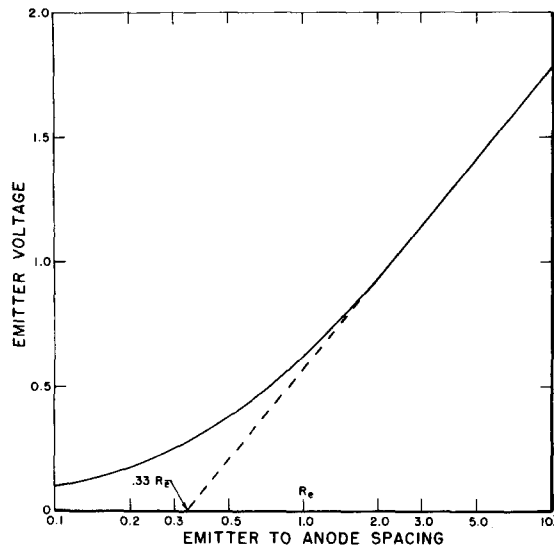

FIG. 15. Theoretical relationship between emitter voltage and emitter to anode spacing [Eq. (4)] obtained from the solution of Laplace's equation and using prolate–spheroidal coordinates. Emitter is a hyperboloid of radius R_e. When the emitter spacing is plotted logarithmically in units of R_e, the straight line portion of the curve at large spacings can be extrapolated until it intersects the abscissa at $0.33R_e$. Thus, the radius of an emitter can be obtained directly from such a plot.
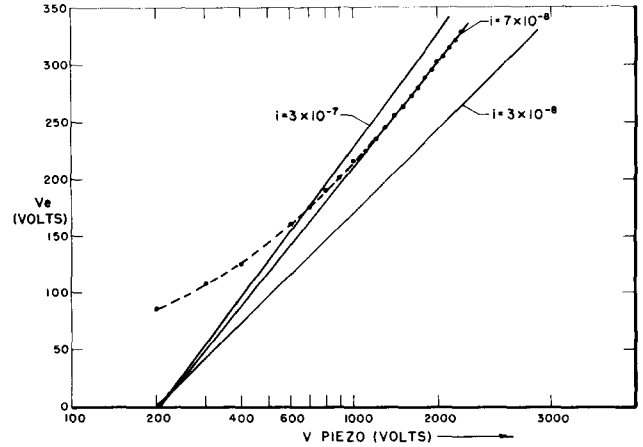

FIG. 16. Experimental curves corresponding to Fig. 15 for three different currents. Since solutions of Laplace's equation are independent of current density, all three curves extrapolate to the same piezo voltage, corresponding to an emitter radius of 8100 Å. Emitter radius $= R_e$; $R_e = 3 \times 208 \times 13.0 = 8100$ Å.

ordinate is the emitter voltage which results when $E_0 = 1$. When the straight line portion of this curve is extrapolated to zero emitter voltage, the corresponding emitter to anode spacing is $0.33R_e$. Thus, the radius of the emitter can be obtained directly from a plot of V vs log of emitter spacing.

An example of three such curves for three different emission currents is given in Fig. 16. The data points are only shown for the center curve. The radius is calculated in Fig. 16 by multiplying the X intercept by three times the d factor for the piezo stack (13 Å/V). It can be shown by manipulating the above equations that the field strength is relatively constant between the emitter and the anode in the region near the apex when the emitter is a small fraction of a radius away from the surface. This is sometimes referred to as the "parallel plate" region. In this region, when the field at the emitter is fixed by the constant current, the emitter voltage is a linear function of the emitter to anode spacing, which is called the "parallel plate effect." In fact, the emitter voltage change per unit distance is the value of the electric field. It is assumed that the emitting area does not change substantially over the range of the measurement.

In the experiments which will be compared with the Fowler–Nordheim theory, and in the following tunneling experiments, the servo loop and scanning piezos were disconnected and a carefully regulated variable voltage was applied to the altitude piezo in order to move the emitter very close to the surface. Figure 17 shows the emitter to anode voltage as a function of piezo voltage (distance) for an unusual situation where the emitter has previously contacted the surface, resulting in flattening of the emitter apex. After recleaning the emitter by annealing, this resulted in a long linear region for the curve and an excellent opportunity to determine the field strength at the surface of the emitter. The structure in the curves is due to
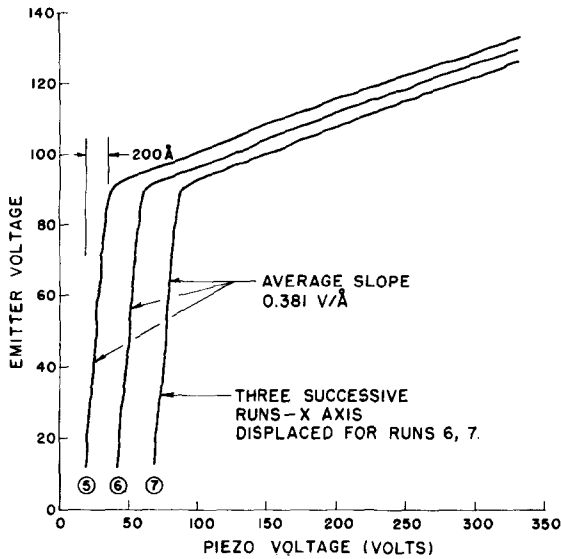
FIG. 17. Emitter voltage vs piezo voltage. The slope of the straight line portion of the curve close to the surface (left-hand side) gives the field strength directly, since the piezo moves 13.0 Å/V. The average field strength is 0.381 V/Å.

the individual wires in the 10 turn potentiometer used to vary the piezo voltage in order to bring the emitter safely in to the surface from a considerable distance. The total excursion over which the field was measured only amounted to 200 Å or 1/40 of the emitter radius. The field strength determined from Fig. 17 is 0.381 V/Å. This can then be used in a Fowler–Nordheim plot to compare theory and experiment, since the field strength associated with one current has been measured.

The Fowler–Nordheim equation can be written in the following logarithmic form[9]:

$$\log\frac{i}{E_0{}^2}=\log\left(1.54\times10^{-6}\frac{A}{\phi_0{}^2 t^2(y)}\right)$$
$$-\left(\frac{6.83\times10^{-7}\phi_0{}^{\frac{3}{2}}v(y)}{E_0}\right), \quad (5)$$

where i is the field emission current, E_0 is the field strength at the emitter apex in volts per centimeter, A is the effective area in square centimeters, ϕ_0 is the emitter work function in electron volts and $\phi(Y)$ and $t(Y)$ are slowly varying elliptic functions. The intercept of the Fowler–Nordheim plot is the first term on the right of Eq. (5). The slope is obtained by taking the derivative of Eq. (5) with respect to $1/F$ and is given by[9]

$$m=0.296\phi_0{}^{\frac{3}{2}}s(y). \quad (6)$$

The Fowler–Nordheim plot associated with the emitter whose field strength was determined in Fig. 17 is shown in Fig. 18. Application of Eqs. (5) and (6) yields the following values: $\phi=4.60$ eV, $A=19\times10^{-10}$ cm^2.

The average work function at the apex of a tungsten emitter is somewhat higher than the over-all average work function for tungsten due to the presence of the high work function (110) region at the apex. Thus, the measured value of 4.60 eV is very reasonable. After accounting for the fact that the Fowler–Nordheim data were taken when the 8100 Å emitter was only about 1000 Å above the surface, the effective emitting area determined from the intercept of the Fowler–Nordheim plot ($A=19\times10^{-10}$ cm^2) implies an approximate emitter radius of 7000 Å. This is in excellent agreement with the measured value of 8100 Å. The effective emitting area was determined from a scale drawing of the emitter and surface, by estimating the contribution to the emitter current from different portions of the emitter apex.

This technique could be used to test the validity of the Fowler–Nordheim equation if certain improvements were made in the experimental technique: (1) The mechanical stability of the instrument would have to be improved; (2) a really flat anode surface would have to be provided; and (3) a known, uniform work function emitter would have to be employed. The above experiment demonstrates that the Fowler–Nordheim equation adequately describes the emission process in the present instrument.

V. METAL–VACUUM–METAL (MVM) TUNNELING

When the field emission probe is sufficiently close to the surface so the potential barrier through which the electrons must tunnel is influenced by the image potential at the anode surface, then the Fowler–Nordheim equation no longer describes the emission process. Still closer to the surface, when electrons from the emitter tunnel to states just above the Fermi energy in the anode material, the process becomes MVM tunneling, a special case of thin film
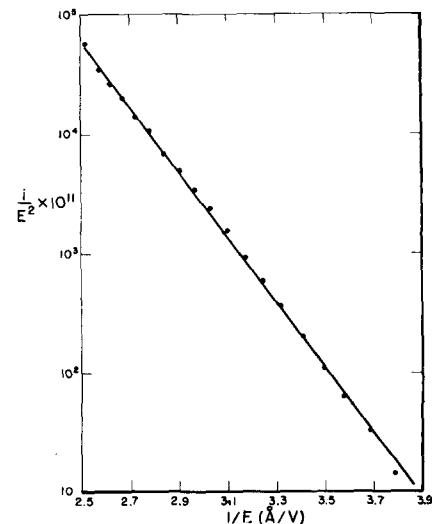

FIG. 18. Fowler–Nordheim plot taken with emitter spacing of about 1000 Å. The field strength was determined from Fig. 17.

tunneling. Simmons has derived a general expression for the relationship between the current density and the applied voltage over the full range from field emission to MVM tunneling.[10] Figure 19 is the potential energy diagram defining the parameters used in Simmons' theory. The most general expression for current density, applicable to potential barriers which include the image potentials at both surfaces, is given by[10]

$$J = [e/2\pi h(\beta \Delta S)^2]$$
$$\times \{\bar{\phi} \exp(-A\bar{\phi}^{\frac{1}{2}}) - (\bar{\phi}+eV) \exp[-A(\bar{\phi}+eV)^{\frac{1}{2}}]\}, \quad (7)$$

where $A = 4\pi\beta\Delta S(2m)^{\frac{1}{2}}/h$, $\beta \simeq 1$,

$$\bar{\phi} = \frac{1}{\Delta S} \int_{S_1}^{S_2} \phi(x)dx,$$

$\phi(x)$ is the potential energy of an electron between the two metal surfaces, $\bar{\phi}$ is the mean value of the potential between S_1 and S_2, m_e is the electron mass, V is the potential between the two electrodes, and the other symbols are defined in Fig. 19. In the MVM range where $eV \ll \phi_0$, Eq. (7) becomes

$$J = [(2m_e)^{\frac{1}{2}}/\Delta S](e/h)^2\bar{\phi}^{\frac{1}{2}}V \exp(-A\bar{\phi}^{\frac{1}{2}}). \quad (8)$$

This equation gives the expected linear dependence between current density and applied voltage, in contrast to the exponential character of Fowler–Nordheim tunneling.

It is appropriate at this point to describe the qualitative difference between the two types of emission. In the Fowler–Nordheim region, the potential barrier is lowered by increasing the applied voltage, resulting in an exponential increase in current density. Since all electronic states are available on the vacuum side of the barrier, the current is not affected by the density of states on that side. In MVM tunneling, there is only a narrow range of available electronic states on the positive electrode, and it is the increase in the number of available states which causes the current density to increase linearly with applied voltage. Changes in the potential barrier have little effect. Thus,
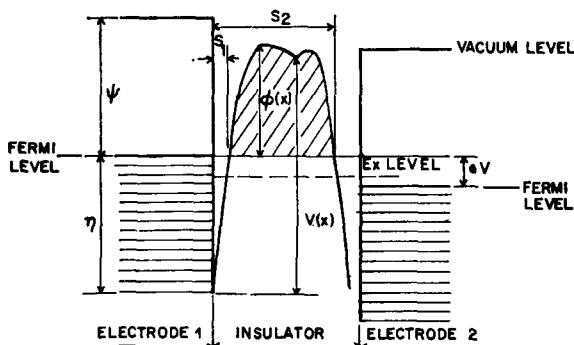

FIG. 19. Potential energy diagram for an electron between two conducting electrodes (after Simmons[10]). In MVM tunneling the insulator is vacuum.
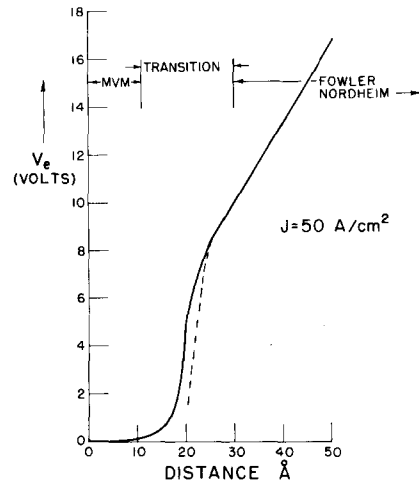

FIG. 20. Theoretical emitter voltage vs distance curve (solid line) showing the Fowler–Nordheim region, the intermediate region, and the MVM region. The dotted line depicts our experience of a rapid drop in voltage when the emitter voltage reaches about 6–8 V. The steep portion of the curve can be used to determine when the emitter is a fixed distance, say 20 Å, from the surface.

two different processes are dominating in the two regions, which means that an entirely different kind of information is obtained from experiments in the two different regions. Since the electrode materials are the same in both cases, and since the geometries of both experiments are directly related, it should be possible to obtain new kinds of information from concurrent experiments in the Fowler–Nordheim and MVM regions.

Equations (7) and (8) predict an extremely strong dependence of current density on electrode spacing. Slight changes in spacing or jumps during adjustment can cause catastrophic loss of the emitter. Experimentally, this is avoided by employing a constant current mode of operation and measuring the interelectrode voltage versus distance. For this reason, a theoretical curve has been calculated from Eq. (7) for a fixed current density. Figure 20 is a plot of the voltage needed to maintain a constant current density of 50 A/cm² versus emitter to anode spacing. The linear Fowler–Nordheim region has a slope of 0.33 V/Å. A sharp drop in the emitter voltage occurs below 25 Å, and below 10 Å only millivolts are needed. The dashed curve does not represent actual data but rather depicts our experience, when decreasing the spacing, of being able to reduce the emitter potential to about 8 V and then suddenly observing a precipitous drop in potential to less than 1 V. This effect has metrological applications in that it is possible to use this device as a noncontacting probe capable of determining the true position of the surface within about 3 Å (one atom layer). The sudden drop in the curve is also responsible for the abrupt increase in servo loop gain for emitter spacings near 20 Å as shown in Fig. 6.

It would be highly desirable to be able to operate the field emission probe and the Topografiner in an atmosphere
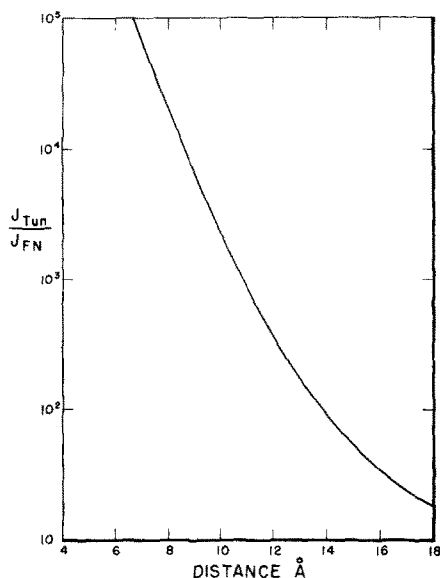
FIG. 21. Calculated ratio of tunneling current density to Fowler–Nordheim predicted current for a fixed field at the emitter of 0.3 V/Å.

of air, nitrogen or rare gas rather than in high vacuum. All attempts to operate in other than high vacuum have failed. As soon as electron emission occurs, the emitter shorts to the anode, presumably due to some sort of high current density, low voltage discharge.

It is also of interest to consider the way in which the MVM tunnel current deviates from the current predicted from Fowler–Nordheim theory as the spacing decreases. Plummer has programmed a numerical calculation of the tunnel current through barriers with special features related to surface adsorbed atoms.[11] This program has been used to calculate the ratio of MVM to Fowler–Nordheim current versus distance for an emitter field strength of 0.3 V/Å and a work function of 4.5 eV. The results, shown in Fig. 21, verify that MVM tunnel current makes an important contribution at about 20 Å and has completely dominated the FN predicted current by 10 Å.

In spite of all the precautions that were taken to minimize shake and acoustical coupling in the experiment, it was necessary to wait for a time when the building air conditioning was off, and to operate the experiment remotely, before MVM tunneling could be measured. The elevation piezo was biased within a few tens of angstroms of the surface with a high voltage power supply and then a second, low voltage power supply was used for fine positioning in angstrom steps. The total piezo voltage was measured with a digital voltmeter with a precision of 0.1 V, corresponding to an emitter motion of 1.3 Å. Mechanical vibrations on the angstrom level limited positioning control to the angstrom level. After moving the

emitter to within 10–30 Å of the surface, the emitter to surface voltage was scanned over a carefully limited range. The emission current was then measured with an electrometer and the current-voltage characteristic was plotted with an $X-Y$ recorder. The results are shown in Fig. 22. Three emission regions have been measured: (1) the lower (closest) limit of the Fowler–Nordheim region, (2) an intermediate spacing, and (3) near the upper limit of the MVM region. The spacings were determined from the current density and the Fowler–Nordheim and MVM theories. The MVM tunneling resistivity $\sigma(=V/J)$ is approximately 4×10^{-3} ohm cm^2. The current–voltage characteristic is linear in the MVM region as expected.

A new instrument for MVM studies is now being tested. Elimination of the scanning system resulted in a more rugged device. Coarse adjustment of the emitter spacing is made with a helium operated, thick walled diaphragm so that the unit can be operated in a cryostat. Further precautions against shake and vibration will be needed before precision experiments can be performed.

There are many applications for MVM studies. Tunneling between single crystal electrodes with clean, well characterized surfaces will be possible. The theory of MVM tunneling could be tested in a very direct way. Experiments which require variation of electrode spacing such as "Fisk modes"[12] could be investigated. Lambe and Jaklevic have shown that inelastic tunneling can be used to study the vibrational spectra of molecules imbedded in an oxide matrix.[13] MVM tunneling could be used to study the vibrational spectra of atoms and molecules adsorbed on clean, well characterized single crystal surfaces. Other applications abound.
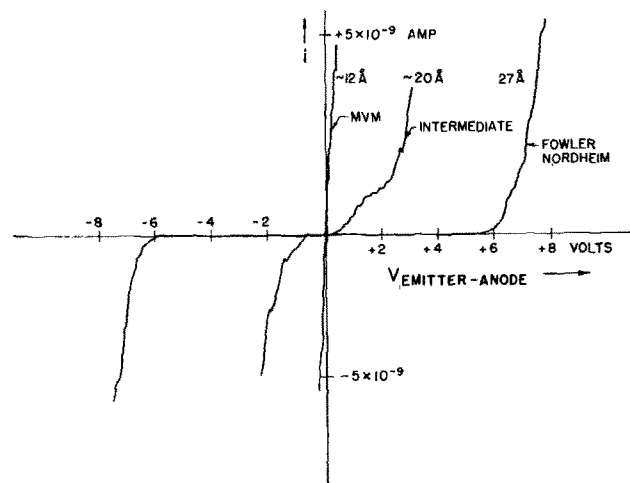

FIG. 22. Tunneling current vs voltage for three different emitter spacings. Note that the MVM tunneling characteristic is a straight line. Tungsten emitter, platinum anode; area≃10^{-9} cm^2; J_{max} ≃50 A/cm^2.

VI. COMPARISON OF THE PERFORMANCE OF VARIOUS INSTRUMENTS USED TO MEASURE SURFACE TOPOGRAPHY

The usefulness of an instrument for measuring surface topography depends on its ability to measure simultaneously the horizontal and vertical separation between two points. For the purpose of comparing the performance of various instruments in this application, the "topographic resolution" is hereby defined as the product of the horizontal and vertical resolution of an instrument. Table I[4] shows the topographic resolution for the transmission and scanning electron microscopes, the Tolansky optical interference microscope, the mechanical stylus instruments, and the Topografiner. All resolutions are estimates of practical working resolutions in measuring topography rather than the best achieved resolution under special conditions. The vertical resolution for the TEM and the SEM are based on sterometric measurements of surface profiles. Note that all instruments appear to have a working topographic resolution of approximately 100 000 Å². This appears to be a practical rather than a fundamental limitation.

VII. FEATURES PLANNED FOR PROTOTYPE TOPOGRAFINER

The present study constitutes the completed feasibility study for the Topografiner. The final horizontal resolution remains an undetermined property of the instrument. The prototype, which is presently under design, will include certain desirable characteristics for an instrument which is generally useful in the measurement of surface microtopography. The scan range, or area covered by the topographic map must be substantially increased, perhaps to cover a 0.254 mm square area. In addition, it should be possible to move from one area to another without breaking vacuum. The vacuum pumpdown time must be short so that specimens can be quickly changed. Further improvement in the servo loop is necessary to improve stability and accuracy.

A data aquisition system must be designed to accommodate the unusually high information density associated with this instrument. For example, if the horizontal resolution were 254 Å (1 μ in.) and 10^4 data points were obtained per scan, then a 100 scan topographic map would contain 10^6 data points. If data are acquired at the rate of 10^3 points/sec, a single mapping would take 17 min.

TABLE I. Topographic resolution of instruments used to measure surface microtopography (transmission electron microscope, scanning electron microscope, Tolansky optical interference microscope, mechanical stylus instruments, and the Topografiner). Topographic resolution for all instruments is about 100 000 Å².

Instrument	Approximate vertical res. (Å)	Approximate horizontal res. (Å)	Topographic resolution, horizontal ×vertical res. (Å²)
TEM	1500	50	75 000
SEM	1500	100	150 000
Optical interference	5	25 000	125 000
Stylus instrument	25	10 000	250 000
Topografiner	30	4 000	120 000

The scanning electron microscope encounters the same sort of data acquisition problem.

The search continues for an emitter which remains sharp and is less sensitive to ambient gas. It is vital to the development of a really useful and well understood instrument that concurrent surface science investigations with the device continue to be conducted. Some suggested experiments were mentioned above.

ACKNOWLEDGMENTS

[1] Symposium on the Science of Ceramic Machining and Surface Finishing, National Bureau of Standards, Gaithersburg, Md., 1970.
[2] W. R. Hunter, J. Opt. Soc. Amer. 55, 1197 (1965); A. Engelsrath and E. V. Loewenstein, Appl. Opt. 5, 565 (1966); H. E. Bennett and J. P. Porteus, J. Opt. Soc. Amer. 51, 123 (1961).
[3] E. G. Loewen, J. Phys. E 3, 953 (1970).
[4] R. D. Young, Phys. Today 24, 42 (Nov. 1971).
[5] From the Greek word τοπογραφειν—"to describe a place."
[6] R. D. Young, Rev. Sci. Instrum. 37, 275 (1966).
[7] W. J. Osterkamp, Philips Res. Rep. 3, 58 (1948).
[8] A. M. Russell, J. Appl. Phys. 33, 970 (1962).
[9] R. H. Good and E. W. Muller, Handbuch der Physik (Springer, Berlin, 1956), Vol. XXI.
[10] J. G. Simmons, J. Appl. Phys. 34, 1793 (1963).
[11] E. W. Plummer and R. D. Young, Phys. Rev. B 1, 2088 (1970).
[12] Fisk modes involve an excess tunneling current in the presence of an external magnetic field. The peak in current is related to voltage, magnetic field strength, and spacing—see Langenburg et al., Proc. IEEE 54, 560 (1966).
[13] L. Lambe and R. C. Jaklevic, Phys. Rev. 165, 821 (1968).